Environmental Science & Technology

pubs.acs.org/est

Article

Oxygenated Aromatic Compounds are Important Precursors of Secondary Organic Aerosol in Biomass-Burning Emissions

Ali Akherati, Yicong He, Matthew M. Coggon, Abigail R. Koss, Anna L. Hodshire, Kanako Sekimoto, Carsten Warneke, Joost de Gouw, Lindsay Yee, John H. Seinfeld, Timothy B. Onasch, Scott C. Herndon, Walter B. Knighton, Christopher D. Cappa, Michael J. Kleeman, Christopher Y. Lim, Jesse H. Kroll, Jeffrey R. Pierce, and Shantanu H. Jathar*

Cite This: *Environ. Sci. Technol.* 2020, 54, 8568–8579

Read Online

ACCESS | Metrics & More | Article Recommendations | Supporting Information

ABSTRACT: Biomass burning is the largest combustion-related source of volatile organic compounds (VOCs) to the atmosphere. We describe the development of a state-of-the-science model to simulate the photochemical formation of secondary organic aerosol (SOA) from biomass-burning emissions observed in dry (RH <20%) environmental chamber experiments. The modeling is supported by (i) new oxidation chamber measurements, (ii) detailed concurrent measurements of SOA precursors in biomass-burning emissions, and (iii) development of SOA parameters for heterocyclic and oxygenated aromatic compounds based on historical chamber experiments. We find that oxygenated aromatic compounds, including phenols and methoxyphenols, account for slightly less than 60% of the SOA formed and help our model explain the variability in the organic aerosol mass (R^2 = 0.68) and O/C (R^2 = 0.69) enhancement ratios observed across 11 chamber experiments. Despite abundant emissions, heterocyclic compounds that included furans contribute to ∼20% of the total SOA. The use of pyrolysis-temperature-based or averaged emission profiles to represent SOA precursors, rather than those specific to each fire, provide similar results to within 20%. Our findings demonstrate the necessity of accounting for oxygenated aromatics from biomass-burning emissions and their SOA formation in chemical mechanisms.

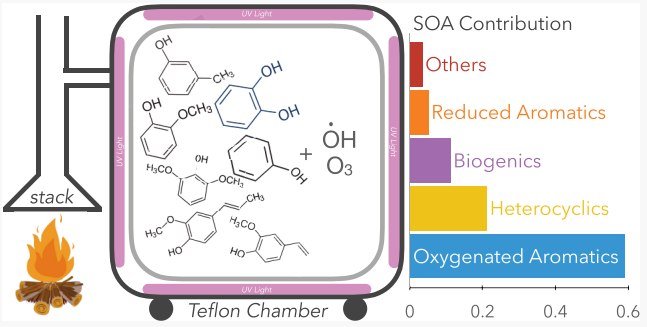

1. INTRODUCTION

Volatile organic compounds (VOCs) participate in photochemical reactions to form secondary organic aerosol (SOA), which accounts for a significant fraction of the submicron atmospheric aerosol mass.[1] Biomass burning, which includes wildfires, prescribed burning, agricultural fires, and residential wood combustion, is the largest combustion-related source of VOCs to the atmosphere.[2−4] However, the contribution of biomass burning to the regional and global SOA burden is quite uncertain,[5] and consequently, the impacts of biomass-burning aerosols on climate, air quality, human health, and visibility[6−8] are uncertain as well. There is a need to better understand the precursors and formation pathways of SOA from biomass-burning sources.

Laboratory experiments performed on biomass-burning emissions, using environmental chambers and oxidation flow reactors, have shown that VOC oxidation results in SOA production and an enhancement in OA mass.[9−13] In instances where the OA mass increased with photochemical aging, the observed SOA production in these experiments varied substantially, with SOA production between zero to six times the primary aerosol emissions. Although some prior work has found it challenging to explain the variability in the SOA produced across different fires, these studies have concluded that precursors, such as alkanes and single-ring aromatics that are important for fossil fuel combustion, contribute little to the measured SOA mass.[12,14,21] Thus, an improved understanding of the VOCs responsible for biomass burning-related SOA is needed.

Detailed speciation of VOCs in biomass-burning emissions is now available through measurements using one- and two-dimensional gas chromatography−mass spectrometry (GC/MS)[15−19] and chemical ionization mass spectrometry (CIMS).[20−24] By linking the detailed VOC speciation to the laboratory-measured SOA formation, several studies have attributed a substantial fraction of the SOA mass to a few

Received: March 4, 2020
Revised: June 19, 2020
Accepted: June 19, 2020
Published: June 19, 2020

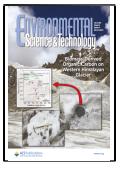

https://dx.doi.org/10.1021/acs.est.0c01345
Environ. Sci. Technol. 2020, 54, 8568–8579

VOC classes of SOA precursors: monoterpenes (e.g., α-pinene), oxygenated aromatics (e.g., phenols), heterocyclic compounds (e.g., furans), and polycyclic aromatic hydrocarbons (PAHs, e.g., naphthalene).[12,21,25] Ahern et al.[12] found monoterpenes to be important for two conifers (i.e., black spruce and ponderosa pine) and furans to be important for grasses (i.e., wiregrass) while Bruns et al.[21] and Stefenelli et al.[25] found oxygenated aromatics and PAHs to be important for SOA from wood stoves. Lim et al. (2019) found tight correlations between the SOA produced and the initial VOC mass, with stronger correlations observed for VOCs more volatile than monoterpenes. These earlier studies suggest that the dominant SOA precursors vary widely based on the fuel and there is a continued need to better understand these precursors across the diversity of fuel types found within the broad source category of biomass burning.

Finally, studies that have modeled SOA formation from biomass-burning emissions in laboratory experiments have not systematically accounted for the influence of vapor losses to the chamber walls,[26−28] multigenerational aging,[29] or kinetic gas/particle partitioning,[30] all of which could influence SOA formation and the interpretation of the chamber data. It is likely that some, if not all, of the differences between earlier studies could be attributed to differences in the experimental methods (e.g., aging time scales) and artifacts (e.g., particle and vapor wall loss rates). There is a need to use models that simulate the detailed physicochemical evolution of the OA mixture and account for experimental artifacts.

In this work, we develop and use a coupled chemistry−thermodynamics−microphysics organic aerosol model to simulate the formation and composition of SOA from new chamber experiments performed on biomass-burning emissions representative of those found in the western US. The primary finding of this work is that oxygenated aromatics are important precursors of SOA formation in chamber experiments performed on biomass-burning emissions.

2. MATERIALS AND METHODS

2.1. Environmental Chamber Measurements. We performed a total of 11 photo-oxidation experiments using the Colorado State University (CSU) 10 m^3 Teflon environmental chamber on emissions from six western US fuels (Ponderosa pine, Lodgepole pine, Douglas fir, manzanita, Engelmann spruce, or subalpine fir), as part of the FIREX (Fire Influence on Regional and Global Environments) laboratory campaign conducted at the Fire Sciences Laboratory in Missoula, MT, in 2016.[31,32] Some fuels were studied in multiple experiments (e.g., Ponderosa pine) while some were studied only once (e.g., Engelmann spruce). Details for all 11 chamber experiments are provided in Table S1. Briefly, a known mass of a single fuel (298−4376 g) placed on a concrete pallet was electrically ignited and the smoke from the fire was diverted into a large stack. Smoke from the stack was drawn and injected into the chamber and irradiated with UV-A lights (32 W × 80 = 2.6 kW) to simulate photochemical oxidation. Five of the chamber experiments were performed under high NO_X conditions (>400 ppbv) with HONO added as an OH precursor. Three experiments were performed under modest NO_X conditions (2−20 ppbv) with H_2O_2 added as an OH precursor; NO_X in these experiments was limited to that generated by the fire. One experiment was performed with UV lights only (no intentional addition of HONO or H_2O_2), and two experiments used ozone (O_3) as an oxidant (~400 ppbv). During the O_3 experiment, oxidation was first performed with O_3 in a dark chamber, and after slightly more than 2 h, the UV lights were turned on.

A high-resolution aerosol mass spectrometer (HR-AMS) was used to estimate OA mass concentrations and the elemental composition (e.g., O/C ratio). The raw OA mass concentrations were corrected for losses and artifacts in the HR-AMS using a scaling factor (SF), which was determined by comparing measurements of nonrefractory aerosol from the HR-AMS to those estimated from measurements made using a scanning mobility particle sizer (SMPS) and single particle soot photometer (SP2). The SF accounts for instrument-specific factors, including transmission, collection, and ionization efficiencies (see the Supporting Information Section "Scaling Factor Calculation"). We also used the composition-dependent collection efficiency (CDCE) approach proposed by Middlebrook et al. (2012) to correct the OA mass concentrations but this approach seemed to produce similar results to those from the use of the SF. Following Ahern et al.,[12] suspended OA mass concentrations were corrected for particle wall losses by assuming that the loss of OA mass at a mass-to-charge ratio of 95.086067 ($C_7H_{11}^+$), which was assumed to be a nonvolatile and nonreactive marker for POA, was purely from particle losses to the walls. These corrections resulted in two estimates for OA mass concentrations assuming: (i) SOA vapors only condensed on the suspended particles (w = 0) and (2) SOA vapors condensed on both the suspended particles and the particles deposited on the walls (w = 1).[28,33] The central estimate in the particle-wall-loss-corrected OA mass concentrations was calculated as an average of these estimates. The uncertainty was approximated by assuming that the two estimates were separated by four standard deviations. For simplicity, the particle-wall-loss-corrected OA mass concentration at lights on was defined as POA and any increase in OA mass was defined as SOA. We assumed that particle-wall-loss-corrected POA mass concentrations remained constant during the experiment; more details about this assumption are discussed in "Treatment of POA" below in Section 2.2. We assumed an uncertainty of 28% on the O/C measurements based on previous laboratory work performed with the HR-AMS.[34]

The modeling relied on OH estimates and O_3 measurements to determine the oxidation chemistry of the SOA precursors. The OH concentrations and exposure were estimated by tracking the decay of deuterated butanol (D9) as measured using a quadrupole proton transfer reaction mass spectrometer (PTR-MS).[35,36] O_3 was directly measured with a reference instrument. We used the number size distributions measured using the SMPS to determine the initial particle size distributions at the beginning of the experiment.

2.2. SOM-TOMAS Modeling. We developed the statistical oxidation model-two moment aerosol sectional (SOM-TOMAS) model to simulate the chemistry, thermodynamic properties, and kinetic gas/particle partitioning of SOA produced during photo-oxidation of biomass-burning emissions. A detailed description of the SOM and TOMAS models can be found in earlier work.[26,37−39] Briefly, the SOM uses a carbon−oxygen grid to track the chemical evolution of the gas- and particle-phase species arising from VOC oxidation. Each cell in the carbon−oxygen grid is a model species that represents the average properties of the oxidation products with the same carbon (N_C) and oxygen (N_O) number. All properties of each model species (e.g., reactivity (k_{OH}) and

https://dx.doi.org/10.1021/acs.est.0c01345
Environ. Sci. Technol. 2020, 54, 8568−8579

volatility (C^*)) are expressed in terms of N_C and N_O. The following six parameters determine the formation, evolution, and thermodynamic properties of the oxidation products in a SOM grid: (i–iv) p_1–p_4, the yields of four functionalized products that add one, two, three, and four oxygen atoms to the carbon backbone, respectively; (v) m_{frag}, the parameter that characterizes the fragmentation probability, $P_{frag} = (O: C)^{m_{frag}}$; and (vi) ΔLVP, the decrease in the saturation vapor pressure (or C^*) of the model species per addition of an oxygen atom. The SOM has been previously used to model SOA formation from individual VOCs,[26,37] VOC mixtures,[28] engine emissions,[44] and precursors in an urban air shed.[29,43,76] The SOM and TOMAS models are coupled in that the particle-phase species in SOM are tracked in the TOMAS size sections. TOMAS in our setup has 36 size sections spanning dry diameters of approximately 3–10,000 nm. In each size section, TOMAS tracks the number of particles and the mass of each SOM model species in the particle phase. In this work, TOMAS simulates coagulation between size sections and kinetic condensation/evaporation of mass between the particle and vapor phases for all SOM model species.

2.2.1. SOA Precursors. Koss et al.[23] used a proton transfer reaction–time of flight–mass spectrometer (PTR-ToF-MS) to measure stack emissions of ∼150 unique hydrocarbons and lightly oxygenated gas-phase organic compounds and ∼370 partially speciated gas-phase organic compounds from 57 separate fires during FIREX. The PTR-ToF-MS was able to identify molecules with up to 4 oxygen atoms per molecule and up to an O/C ratio of 2. Partially speciated VOCs were those where Koss et al.[23] could not determine an exact speciation and assumed that the detected species only comprised C, H, and O. Alkanes and partially speciated compounds larger than C_{10}, reduced and oxygenated aromatics, heterocyclics, and biogenics were considered to form SOA in this work. Altogether, 86 speciated VOCs and 61 partially speciated VOCs that were lumped by carbon and oxygen number were modeled to form SOA. Concentrations of SOA precursors measured in the stack were averaged over the duration of the fire and ratioed with acetonitrile to calculate fire-specific emission ratios (i.e., VOC_i/acetonitrile). Acetonitrile was chosen over other inert tracers such as CO because the background (room) concentrations of acetonitrile were relatively much lower than those in the stack. The PTR-ToF-MS instrument measured emissions in the stack and not in the chamber (except for Fire007). Hence, initial concentrations of the SOA precursors at the beginning of the chamber experiment were calculated by multiplying the stack-based emission ratios with the acetonitrile concentrations measured using a different quadrupole PTR-MS that sampled from the chamber.[40,41] Based on simultaneous measurements made during FIREX in a different chamber across 30 individual experiments,[13] we found that the acetonitrile concentrations measured using the quadrupole PTR-MS were 38% higher than those measured using the PTR-ToF-MS (Figure S2), possibly from multiple isobaric interferences from the unit mass resolution of the quadrupole PTR-MS. The initial concentrations of the SOA precursors were scaled by 0.62 to account for this difference. Stack emission data from the PTR-ToF-MS were directly available for five of the 11 chamber experiments. For the remaining, PTR-ToF-MS-derived emission ratios (to acetonitrile) from all fires performed with the same fuel as that used in the chamber experiment were averaged before being used for that particular chamber experiment. Emission ratios for the SOA precursors, lumped by the VOC class, for each of the 11 chamber experiments are presented in Table S2. We also considered the uncertainty reported in the PTR-ToF-MS measurements and examined its influence on model predictions of SOA. Lower- and upper-bound estimates for SOA production due to these uncertainties in the emission measurements were calculated by running two sets of simulations for each experiment, assuming that all SOA precursors were either at their lower or upper bounds, based on the 95th percentile confidence interval documented in Koss et al.[23] The uncertainty varied by VOC (15–100%; 2σ), with lower uncertainties for smaller carbon number VOCs and hydrocarbons and larger uncertainties for larger oxygenated VOCs. The uncertainty in the model predictions for SOA was approximated by assuming that the lower and upper bounds were separated by four standard deviations. We should note that we did not consider the SOA formation from semivolatile organic compounds (SVOCs) emitted by biomass burning[19] and recommend that this be examined in the future.

2.2.2. SOM Parameterizations for Traditional Precursors. Each SOA precursor based on the PTR-ToF-MS data and its reaction with OH/O_3 was modeled explicitly in the SOM-TOMAS model. The parent VOC was allowed to react with OH (for all SOA precursors) and O_3 (biogenic SOA precursors only). In modeling the SOA formation, the 147 (86 + 61) potential SOA precursors were assigned to one of nine surrogate compounds or compound classes: (i) *n*-dodecane, (ii) benzene, (iii) toluene, (iii) *m*-xylene, (iv) naphthalene, (v) isoprene, (vi) α-pinene, (vii) an alkylfuran mixture consisting of 60% dimethylfuran and 40% 2-methylfuran, (viii) phenol and guaiacol, and (ix) syringol; more details can be found in Table S3. This is in line with other approaches[42] and necessary because experimental observations and parameterizations of SOA formation are not available for each individual compound. The SOM parameters for each of these surrogates were developed based on high-NO_X chamber experiments and are listed in Table S4. We chose to use SOM parameters for the high-NO_X chamber experiments because simulations performed with a modified version of the master chemical mechanism (MCM) suggested that the peroxy radicals (RO_2) predominantly reacted with NO in nine of the 11 chamber experiments, even those in which no additional HONO was added;[41] the branching ratio (β) that quantifies the RO_2 fate was calculated for all of the experiments and is presented in Figure S3. Although not definitive, the MCM simulations helped minimize the uncertainty linked to extrapolating the high-NO_X SOA parameters based on single VOC experiments to the biomass-burning experiments analyzed in this work. Alkanes larger than C_{10} were modeled as *n*-dodecane, C_8 and larger single-ring aromatics were modeled as *m*-xylene, all monoterpenes and sesquiterpenes were modeled as α-pinene, and all PAHs were modeled as naphthalene. Although SOA mass yields for the different monoterpenes found in biomass-burning emissions may vary by more than a factor of 2,[16] Ahern et al.[12] showed that the use of α-pinene as a surrogate to model SOA formation from all monoterpenes only marginally changed model predictions. For these traditional SOA precursors, the surrogate choice was similar to that used in previous applications of the SOM[43] and the SOM parameters for these surrogates were corrected for the influence of vapor

https://dx.doi.org/10.1021/acs.est.0c01345
Environ. Sci. Technol. 2020, 54, 8568–8579

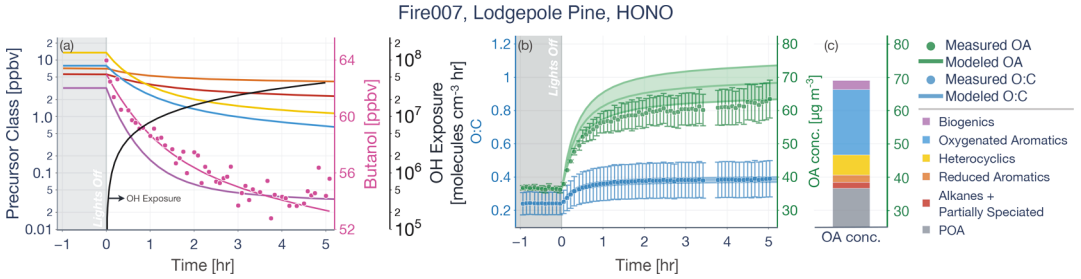

Figure 1. (a) Decay of D9 (deuterated butanol, pink) and VOCs, summed by class, with time and the OH exposure estimated based on the decay of D9; color scheme for VOCs can be found in the legend to the extreme right. (b) Model predictions of OA mass concentrations (green) and O/C ratio (blue) compared with measurements. Both results are for a lodgepole pine experiment performed under high NO_X conditions (Fire007). (c) Bar to the right shows the modeled contributions of POA and precursor-resolved SOA to the end-of-experiment OA.

wall losses based on the loss rates estimated by Zhang et al.[26] ($k_{vap,on}$ = 2.5 × 10^{-4} s^{-1}). Heterocyclic compounds that included furans and substituted furans were modeled using the alkylfuran mixture while oxygenated aromatics, except for syringol, were modeled as phenol or guaiacol (more details in the next paragraph). In the absence of additional information, partially speciated SOA precursors larger than C_{10} were modeled as *n*-dodecane.

The surrogates and SOM parameters used to model the SOA precursors in this work only inform the statistical trajectory for the oxidation chemistry and it is very likely that the surrogate itself and the SOA precursor (as long as they are not identical) have different SOA mass yields.[44] For example, SOA precursors with a carbon number larger than the surrogate will have higher SOA mass yields and vice versa. This approach has been found to work well[37] and is generally consistent with observations for alkane[11,77,78] and alkene (including biogenic) VOCs.[79−81] The SOA mass yields for C_8 and larger single-ring aromatics do not seem to vary strongly with carbon number so this approach likely overestimates the SOA contribution from these precursors. There is limited evidence on how SOA mass yields for heterocyclics and oxygenated aromatics vary by the carbon number. As discussed in the next section, the SOM parameters used to model the SOA formation from heterocyclics and oxygenated aromatics were determined in a way to approximately account for the influence of the carbon number on the SOA mass yields.

2.2.3. SOM Parameterizations for Heterocyclics and Oxygenated Aromatics. Recently, He et al.[28] performed high-NO_X chamber experiments with an alkylfuran mixture (60:40 mixture of 2-methylfuran and dimethylfuran by mass) and developed SOM parameters (i.e., p_1−p_4, m_{frag}, and ΔLVP described earlier) to simulate the SOA formation and O/C ratio from that mixture; these parameters were corrected for vapor wall losses using an estimated vapor wall loss rate coefficient ($k_{vap,on}$) of 1.28 × 10^{-3} s^{-1} for that specific chamber. Furans and substituted furans account for a substantial fraction of heterocyclic compounds in biomass-burning emissions,[23] and hence, we used the SOM parameters for the alkylfuran mixture, in the absence of SOA mass yield data, to represent the SOA formation from all heterocyclic compounds. SOM parameters for all oxygenated aromatics were developed here using the high-NO_X chamber experiments of Yee et al.[45] for phenol and guaiacol. The chamber SOA mass yields for phenol and guaiacol in Yee et al.[45] were similar to those observed in other experiments performed with phenolic species.[45−51] A single SOM parameter set was able to explain the evolution of the SOA mass concentrations in the phenol and guaiacol experiments when differences in their molecular formulas were accounted for, indicating that the oxidation chemistry of these two species might be similar. A separate SOM parameter set was developed for syringol because the phenol- and guaiacol-based parameters overestimated the SOA formation from syringol by nearly a factor of two. The model-measurement comparisons for the phenol, guaiacol, and syringol experiments are shown in Figure S4. The SOA parameters for the phenolic species slightly underpredicted the O/C values measured for SOA from those species (between 0.8 and 1).[52] The oxygenated aromatics parameters were corrected for the influence of vapor wall losses based on the loss rates estimated by Zhang et al.[26] (k_{vapor} = 2.5 × 10^{-4} s^{-1}) as these experiments were performed in the same chamber.

2.2.4. Treatment of POA. Previous work has found POA from biomass-burning emissions to be semivolatile.[53,54] Bian et al.,[55] based on the results of a kinetic model, argued that the loss of semivolatile POA vapors to the Teflon walls can lead to substantial evaporation of the suspended POA mass in chamber experiments performed on biomass-burning emissions. Hennigan et al.[9] suggested that POA can undergo heterogeneous oxidation on the time scale of a chamber experiment. In contrast to these earlier studies, we did not find evidence for evaporation or photochemical processing of POA during the FIREX chamber experiments. This is consistent with findings from experiments performed with a smaller chamber during FIREX.[56] In at least one experiment where the chamber contents were monitored in the dark for more than an hour, the particle-wall-loss-corrected POA mass concentrations did not vary much (∼2−3%) during the dark period (see Figure 1a for Fire007). This could mean that the POA was primarily composed of sufficiently low-volatility material to not be affected by the loss of semivolatile vapors to the Teflon walls that could lead to evaporation of the suspended POA mass. Alternatively, it is possible that the evaporation rates linked to the loss of semivolatile POA vapors to the Teflon walls were too slow to be observed during the dark period in that experiment. The slow evaporation rates could indicate a mass transfer limitation because of a viscous or semisolid aerosol, which has been previously observed for combustion-related POA.[57,58] Furthermore, particle-wall-loss-corrected concentrations of the OA mass at a mass-to-charge ratio of 60.02113 ($C_2H_3O_2^+$), one that includes contributions from directly emitted compounds such as levoglucosan, mannosan, and galactosan,[9,59−61] did not change much during the photo-oxidation periods for all chamber experiments (Figure S5). This might suggest that POA was not being photochemically processed during our chamber experiments. Based on the

https://dx.doi.org/10.1021/acs.est.0c01345
Environ. Sci. Technol. 2020, 54, 8568−8579

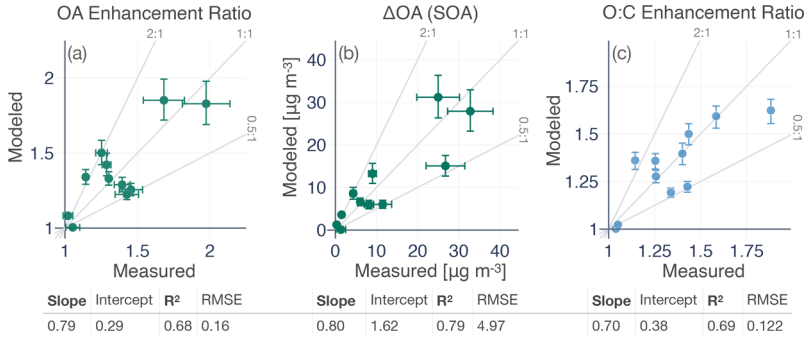

Figure 2. End-of-experiment model-measurement comparison for (a) OA mass enhancement ratios (ratio of final-to-initial particle-wall-loss-corrected OA mass), (b) SOA production ($\mu g\ m^{-3}$), and (c) OA O/C enhancement ratios (ratio of final-to-initial O/C ratios) for all 11 chamber experiments. Statistical metrics based on a linear fit to the model-measurement comparison are presented at the bottom of each panel. rmse = root mean squared error.

available evidence in our specific experiments, we assumed in our simulations that the particle-wall-loss-corrected POA mass concentrations remained constant during the photo-oxidation experiments. Future modeling studies may need to explicitly model the POA volatility and the phase state of OA and their impacts on gas/particle partitioning. This assumption also allowed us to calculate the lower limit of SOA mass produced during the experiment by subtracting the initial POA from the particle-wall-loss-corrected OA mass concentrations. Any loss of POA, either through evaporation or photochemical oxidation, should increase the SOA estimates.

2.2.5. Accounting for Experimental Artifacts. In the SOM-TOMAS model, losses of vapors to the walls of the Teflon chamber are modeled here following Zhang et al.[26] and Krechmer et al.[62] Briefly, the first-order loss rate of vapors to the walls is assumed to be equal to $k_{vap,on}$ and the release of vapors from the walls is modeled using absorptive partitioning theory where the Teflon wall is assumed to have an equivalent mass concentration that varies based on the volatility of the model species (C_{wall} = 16 $\mu g\ m^{-3}$ to 10 mg m^{-3}).[62] Recently, He et al.[28] estimated an average $k_{vap,on}$ of 1.28 × 10^{-3} s^{-1} for the CSU chamber from the observed loss rates of small, electrically neutral particles (<100 nm). In addition to losses of vapors to the chamber walls, vapors were also lost to the flexible aluminum transfer duct that brought smoke from the stack to the chamber (ID ∼20 cm × length ∼20 m, volumetric flow rate of 0.47 $m^3\ s^{-1}$, and residence time of 1.5 s) or in the ejector diluters used to fill the chamber with smoke. To investigate the losses of SOA precursors to the walls of the transfer duct, we compared emission ratios of SOA precursors in the stack to those in the chamber for Fire007 (Figure S6); this was the only experiment where the PTR-ToF-MS sampled from both the stack (during the burn) and the chamber (after the burn and chamber filling were complete). We found that the intermediate-volatile SOA precursors ($10^4 < C^* < 10^6$ $\mu g\ m^{-3}$) were moderately lost in the transfer duct with the largest losses seen for oxygenated aromatics (average of ∼30%). These precursor loss percentages parameterized to C^*, based on the Fire007 experiment, were applied to determine the initial concentrations of SOA precursors for all chamber simulations.

2.2.6. Simulations. We performed the following sensitivity simulations to investigate the influence of model inputs on SOA production: (i) no losses of vapors to the walls of the Teflon chamber, (ii) no losses of SOA precursors to the transfer duct, (iii) no losses of vapors to the walls of the Teflon chamber and no losses of SOA precursors to the transfer duct, (iv) initial concentrations of SOA precursors calculated using a campaign-averaged emission profile, and (v) initial concentrations of SOA precursors calculated using the low- and high-temperature pyrolysis profiles of Sekimoto et al.[24] For (iv), the emission profiles for all 57 fires measured by Koss et al.[23] during the FIREX laboratory campaign were first normalized and then averaged to determine a campaign-averaged emission profile. Sekimoto et al.[24] performed positive matrix factorization on all the emission data measured by Koss et al.[23] and found that two emission profiles, namely, a low- and high-temperature pyrolysis profile, were able to explain the variability in emissions across these 57 fires. In (v), we used the low- and high-temperature pyrolysis profiles identified by Sekimoto et al.[24] and combined them using averaged, experiment-specific low- and high-temperature weights to calculate a fire-specific emission profile. The base, Koss et al. (2018), and Sekimoto et al.[24] emission profiles as an emission ratio with acetonitrile, aggregated by the SOA precursor class, and for all fires analyzed in this work are listed in Table S2.

3. RESULTS

3.1. Example Experiment. In Figure 1a, we show the modeled decay of SOA precursors with time and the measured decay of D9 and the fit used to determine the OH exposure for the chamber experiment performed on emissions from lodgepole pine (Fire007). We left out the measured decay for visual clarity but the model-measurement comparison in SOA precursor decay is shown in Figure S7. In Figure 1b, we show the modeled and measured temporal evolution of the OA mass concentration and O/C ratio for the same experiment. In this experiment, HONO was added as an OH precursor to the chamber, which resulted in high NO_X concentrations (∼900 ppbv at lights on) and a high OH exposure (1.4 × 10^7 molecules h cm^{-3} or 9.3 photochemical hours at an OH concentration of 1.5 × 10^6 molecules h cm^{-3}). The SOM-TOMAS model was able to reasonably reproduce the magnitude and evolution of the OA mass concentration and O/C ratio during the photo-oxidation period. The average-modeled OA mass concentrations were slightly higher than the average-measured OA mass concentrations but with significant overlap of the uncertainty ranges. In contrast, predictions of the average O/C ratio agreed very well with the measurements. Sensitivity simulations performed by gradually decreasing the initial SOA precursor concentrations to match the average-predicted OA mass concentrations with the measurements

https://dx.doi.org/10.1021/acs.est.0c01345
Environ. Sci. Technol. 2020, 54, 8568−8579

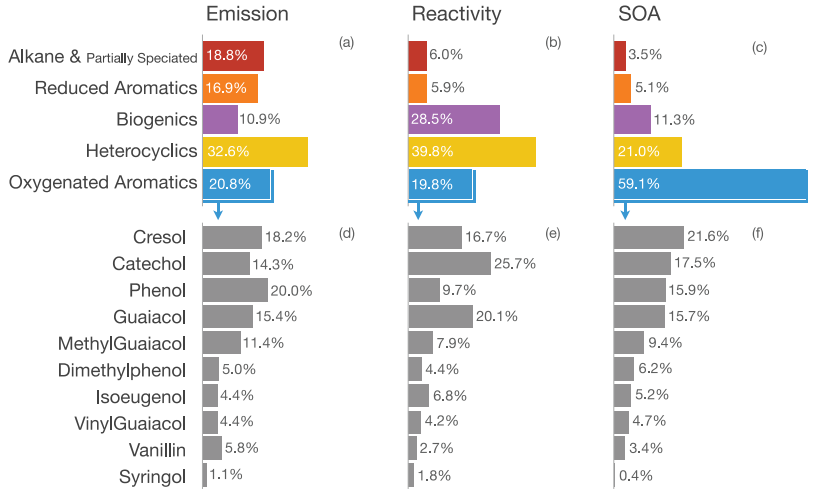

Figure 3. Normalized emissions and OH reactivity of the SOA precursors and their contribution to SOA production for the average of the 11 chamber experiments analyzed in this work. Some of the SOA precursor classes are lumped for clarity (e.g., alkanes + partially speciated, reduced aromatics). Top panels show results for all SOA precursors and bottom panels show results for just the oxygenated aromatic precursors.

resulted in an underprediction of the O/C, highlighting the tight coupling between OA mass concentrations and O/C ratios for the predictions. The use of a constant POA reproduced the flat POA profile measured during the dark period. As shown in the bar chart in Figure 1c, while POA continued to account for a substantial fraction of the aged OA (>50%), the majority of the modeled SOA mass seemed to arise from the oxidation of oxygenated aromatics. Time-series comparisons for OA mass concentrations and O/C ratios for all chamber experiments are shown in Figures S8 through S17.

3.2. Study-Wide Comparison for OA and SOA Mass and O/C. The model-measurement comparisons for the end-of-experiment OA mass enhancement ratio (the ratio of the final-to-initial OA masses), SOA production, and O/C enhancement ratio for all 11 chamber experiments are shown in Figure 2. For most experiments, the model was able to generally track the measured temporal evolution in the OA mass concentrations and O/C ratios (see Figures S8−S17), and hence, we only compared end-of-experiment values in Figure 2. An analogue of Figure 2, but one where the model predictions are compared to the measurements at four different points during each experiment, is provided in the Supporting Information (Figure S18). The SOM-TOMAS model was able to reproduce the OA mass enhancement ratio (Figure 2a) and SOA production (Figure 2b) to within a factor of 2 across all chamber experiments, despite significant differences in the fuel type (pines to shrubs), initial OA loading (10−58 μg m^{-3}), initial seed surface area (120−740 μm^2 cm^3), and OH exposure (<10^6 to 1.4 × 10^7 molecules h cm^{-3} or <1 to ∼10 h of photochemical aging assuming an OH concentration of 1.5 × 10^6 molecules cm^{-3}). For both the OA mass enhancement ratio and SOA production, the model was able to explain 68 and 79% of the observed variability, respectively. The model was able to reproduce the measured enhancement in the O/C ratio and the model explained 69% of the observed variability. We also compared model predictions of the SOA O/C ratio to the measurements. We calculated the SOA O/C ratio for the measurements by assuming that the measured change in the O/C ratio was purely from the condensation of SOA (rather than through the evaporation and/or oxidation of POA). Across the 11 chamber experiments, the model-predicted SOA O/C ratio of 0.64 ± 0.04 was slightly higher than the measurement-derived SOA O/C ratio of 0.58 ± 0.2 (mean ± standard deviation). Because there were significant differences in the model-measurement comparison across experiments, we examined if the model error correlated with any of the input variables (Figure S19). We did not find any strong correlations possibly because there were many more variables than chamber experiments that contributed to differences between experiments. Analysis of a larger dataset might be required to identify deficiencies in the model to simulate certain physical and chemical processes. Overall, the model-measurement comparison for the OA mass enhancement ratio, SOA production, and O/C enhancement ratio indicated that the model was able to represent the majority of the key precursors and processes needed to simulate the OA evolution during photo-oxidation of biomass-burning emissions. We did not model the SOA formation from SVOCs[19] (Hatch et al., 2018) and it is possible that the model performance could be improved if these precursors were considered.

3.3. Precursor Contributions to SOA. The contribution of the different SOA precursors to gas-phase emissions, OH reactivity, and SOA production is shown in Figure 3 as an average over the 11 chamber experiments and results for each individual experiment are shown in Figure S20. Heterocyclic compounds, which were mostly composed of furans and substituted furans, accounted for nearly a third of the SOA precursor emissions by mass while oxygenated aromatics, which were exclusively composed of phenols and methoxyphenols, accounted for a fifth. Altogether, the SOA precursors (excluding the partially speciated compounds) were about 38% of the total VOC emissions (Figure S21a) and, interestingly, similar to SOA precursor fractions found in gasoline, diesel, and aircraft exhaust.[63] As heterocyclic compounds, oxygenated aromatics, and biogenic VOCs have a much higher reactivity with OH relative to alkanes and reduced aromatics,[64] these three classes accounted for almost 90% of the initial OH reactivity linked to SOA precursors. Koss et al.[23] showed that together, these classes accounted for a large fraction (60%) of the total OH reactivity (Figure S21b).

Model predictions suggested that oxygenated aromatics contributed up to 60% of the SOA mass produced in our chamber experiments, despite this class contributing to only a

https://dx.doi.org/10.1021/acs.est.0c01345
Environ. Sci. Technol. 2020, 54, 8568−8579

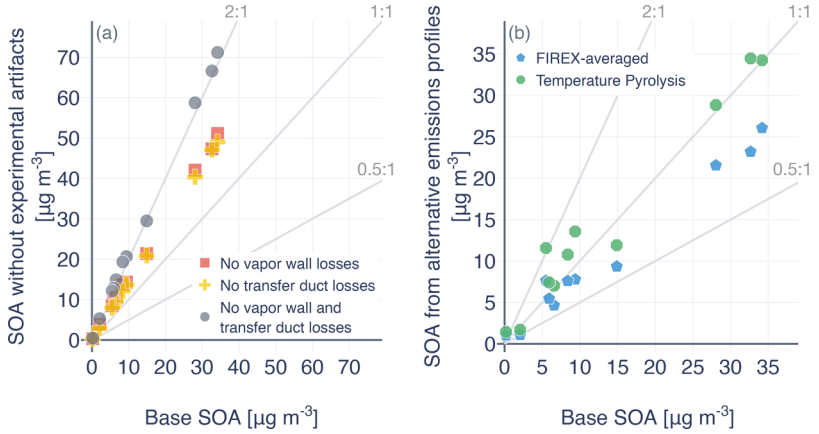

Figure 4. Model predictions of end-of-experiment SOA mass concentrations compared between simulations performed (a) with and without experimental artifacts and (b) with fire-specific and averaged emission profiles.

fifth of the emissions and OH reactivity linked to the SOA precursors. Heterocyclic compounds and biogenic VOCs, respectively, were estimated to contribute ∼20 and ∼10% each to the total SOA mass while alkanes and reduced aromatic compounds made even smaller contributions (<6% each). The heterocyclic compounds did not contribute significantly to SOA production because of their small SOA mass yield,[28,65] despite accounting for a substantial fraction of the emissions and OH reactivity of the SOA precursors. Among the oxygenated aromatics, five species, namely, phenol, cresol, guaiacol, methylguaiacol, and catechol, accounted for slightly less than half of the total SOA and ∼80% of the SOA from oxygenated aromatics. The relative contribution of the different oxygenated aromatics to the emissions, OH reactivity, and SOA production was roughly similar, especially for the five major contributors. This is despite having a slightly different potential to form SOA on account of their different carbon and oxygen numbers.

3.4. Influence of Experimental Artifacts. We investigated the influence of the experimental artifacts, namely, those associated with the transfer duct and chamber walls, on model predictions of SOA. Results from those simulations are shown in Figure 4a, where we compare the SOA predicted without the experimental artifacts to the SOA predicted in the base simulations with artifacts accounted for. Simulations performed without the loss of SOA precursors in the transfer duct resulted in an average increase of 44% in SOA mass concentrations compared to those in the base simulations. The increase was roughly proportional to the 30% increase in initial concentrations of oxygenated aromatics in the simulations where transfer duct losses were not considered. Similarly, turning vapor wall losses off inside the chamber resulted in an average increase of 47% in SOA predictions compared to those in the base simulations. This relative level of increase in SOA mass concentrations appears to be similar to the average increase of 40% estimated previously for several SOA precursors under high NO_X conditions.[26] The vapor-wall-loss effect was smaller than what would be expected given a short gas/wall partitioning time scale (∼13 min). This is because oxygenated aromatics and their oxidation products, on account of their relatively higher OH reactivity, are likely to proceed quickly through the cascade of oxidation reactions to form SOA,[50] which should make the precursors and oxidation products less susceptible to vapor wall losses.[43] When considered together, that is, on turning transfer duct and chamber losses off, the model predicted a combined increase of 105% in SOA mass concentrations. These results imply that in the absence of dilution and similarity in chemistry, photochemical oxidation within biomass-burning plumes should have twice the potential to form SOA as in the chamber.

3.5. Impact of Average Emission Profiles. We simulated the SOA production using two additional approaches to calculate the initial SOA precursor concentrations: (i) campaign-averaged emission profile for fuels found in the western US[23] and (ii) use of the temperature pyrolysis profiles of Sekimoto et al.[24] Both approaches simulate the calculation of an emission profile in the absence of direct measurements. Predictions from these simulations are compared against those from the base simulations in Figure 4b. The use of the temperature pyrolysis profiles produced slightly higher SOA mass concentrations (∼20%) while the campaign-averaged emission profile produced slightly lower SOA mass concentrations (∼20%) when compared to the base simulations. These differences could be attributed to a proportionate increase and decrease in the initial concentrations of oxygenated aromatics and heterocyclics calculated from the emission profiles. These emission profiles are listed in Table S2. These results indicate that, in the absence of direct measurements, averaged or pyrolysis-based emission profiles may be used to determine the SOA precursor concentrations in biomass-burning emissions with the understanding that these may add an additional layer of uncertainty (found to be 20% for the fires investigated in this work) in representing the potential of these emissions to form SOA during photooxidation.

4. DISCUSSION

Although laboratory experiments have typically shown clear evidence for SOA production and an enhancement in OA mass with photochemical aging, field measurements have not observed an enhancement in OA mass with aging in biomass-burning plumes; see Hodshire et al.[27] and references therein. Because oxygenated aromatics have relatively short atmospheric lifetimes with respect to OH, they will, depending on the OH concentrations, rapidly form SOA in the first few hours after emission. If oxygenated aromatics contribute to most of their SOA close to the fire, it might partly explain why aircraft-based measurements, which are limited in how close they can get to the fire (∼15−60 min after emission), do not

https://dx.doi.org/10.1021/acs.est.0c01345
Environ. Sci. Technol. 2020, 54, 8568−8579

consistently show an enhancement in OA mass (i.e., the SOA formation has happened prior to the closest measurement). An additional piece of evidence that oxygenated aromatics might be forming SOA before or close to the first aircraft transect is that, on average, the initial O/C observed in the field on the first transect was higher than the initial O/C in the chamber (and closer to the final O/C observed in the chamber; Figure S22). This however neither agrees with the findings from the smaller chamber during FIREX[66] nor does it explain field observations of an increasing O/C of the OA with age beyond the first transect that could be linked to heterogeneous chemistry.[27,67]

Several studies have hypothesized that the lack of an enhancement in OA mass in the field could be explained if the photochemistry-driven SOA formation was balanced by dilution-driven POA evaporation.[68−70] In this work, based on the available evidence, we assumed that the POA mass concentrations did not vary during the chamber experiment but note that there was very little dilution in our experiments compared to what would be observed in a biomass-burning plume. This hypothesis currently remains untested for field data and any hypothesis testing would need to not only model the SOA formation from oxygenated aromatics and heterocyclic compounds but also model the evaporation kinetics of the POA and subsequent oxidation of the evaporated vapors to correctly interpret the field observations.

In both chamber studies performed during the FIREX laboratory campaign, namely, the data used in this work and the data from Lim et al.,[13] the scaling factor, used to correct the raw OA mass concentrations from the HR-AMS, seemed to vary with photochemical oxidation. In both instances, the scaling factor seemed to decrease with oxidation, which produced a larger correction in the OA mass concentrations as the emissions were aged. In contrast to these studies, Liu et al.[71] found little evidence for the scaling factor changing with time when sampling aerosol from wildfires during the Biomass Burning Observation Project (BBOP). Differences in the laboratory and the field could arise from differences in the relative humidity: mostly dry in the current laboratory case (<20%) but higher in the field (>40%), which may lead to differences in the particle phase state. Regardless, laboratory and field measurements of OA made with an HR-AMS need to be carefully corrected before being used to evaluate models. We note that in sensitivity simulations performed with bounds on the scaling factor (0.5−1), the model measurement comparison did not change dramatically and did not affect the key findings from this work (Figure S23).

One of the limitations of the chamber experiments here was that the experiments were performed under dry conditions (relative humidity <20%) where the only pathway for SOA formation was through gas-phase oxidation followed by partitioning of lower volatility products to the particle phase. In a biomass-burning plume, where the relative humidity is likely to be much higher, oxygenated VOCs such as phenols and furans, which are somewhat water-soluble, could partition into aerosol water and undergo a different chemical fate than that explored in this work.[72−75] The simultaneous, but competing, production of SOA from oxygenated VOCs through gas- and aqueous-phase pathways needs to be better understood in the future.

■ ASSOCIATED CONTENT

Supporting Information

The Supporting Information is available free of charge at https://pubs.acs.org/doi/10.1021/acs.est.0c01345.

Model inputs, model predictions, analysis for individual chamber experiments, and description of SOA precursor emissions and parameters (PDF)

■ AUTHOR INFORMATION

Corresponding Author

Shantanu H. Jathar − *Department of Mechanical Engineering, Colorado State University, Fort Collins 80525, Colorado, United States;* orcid.org/0000-0003-4106-2358; Email: shantanu.jathar@colostate.edu

Authors

Ali Akherati − *Department of Mechanical Engineering, Colorado State University, Fort Collins 80525, Colorado, United States*

Yicong He − *Department of Mechanical Engineering, Colorado State University, Fort Collins 80525, Colorado, United States*

Matthew M. Coggon − *Cooperative Institute for Research in Environmental Sciences, University of Colorado, Boulder 80309, Colorado, United States; Chemical Sciences Division, NOAA Earth System Research Laboratory, Boulder 80305, Colorado, United States;* orcid.org/0000-0002-5763-1925

Abigail R. Koss − *Department of Civil and Environmental Engineering, Massachusetts Institute of Technology, Boston 02139, Massachusetts, United States*

Anna L. Hodshire − *Department of Atmospheric Science, Colorado State University, Fort Collins 80525, Colorado, United States;* orcid.org/0000-0002-5099-3659

Kanako Sekimoto − *Cooperative Institute for Research in Environmental Sciences, University of Colorado, Boulder 80309, Colorado, United States;* orcid.org/0000-0001-9908-9698

Carsten Warneke − *Cooperative Institute for Research in Environmental Sciences, University of Colorado, Boulder 80309, Colorado, United States; Chemical Sciences Division, NOAA Earth System Research Laboratory, Boulder 80305, Colorado, United States*

Joost de Gouw − *Department of Chemistry and Cooperative Institute for Research in Environmental Sciences, University of Colorado Boulder, Boulder 80309, Colorado, United States;* orcid.org/0000-0002-0385-1826

Lindsay Yee − *Environmental Science, Policy, and Management, University of California Berkeley, Berkeley 94720-3114, California, United States;* orcid.org/0000-0001-8965-9319

John H. Seinfeld − *Department of Chemical Engineering, California Institute of Technology, Pasadena 91125, California, United States;* orcid.org/0000-0003-1344-4068

Timothy B. Onasch − *Aerodyne Research Inc., Billerica 01821, Massachusetts, United States;* orcid.org/0000-0001-7796-7840

Scott C. Herndon − *Aerodyne Research Inc., Billerica 01821, Massachusetts, United States*

Walter B. Knighton − *Department of Chemistry, Montana State University, Bozeman 59717, Montana, United States*

Christopher D. Cappa − *Department of Civil and Environmental Engineering, University of California Davis, Davis 95616, California, United States*

Michael J. Kleeman − *Department of Civil and Environmental Engineering, University of California Davis, Davis 95616, California, United States;* orcid.org/0000-0002-0347-7512

https://dx.doi.org/10.1021/acs.est.0c01345
Environ. Sci. Technol. 2020, 54, 8568−8579

Christopher Y. Lim − *Department of Civil and Environmental Engineering, Massachusetts Institute of Technology, Boston 02139, Massachusetts, United States*

Jesse H. Kroll − *Department of Civil and Environmental Engineering, Massachusetts Institute of Technology, Boston 02139, Massachusetts, United States;* orcid.org/0000-0002-6275-521X

Jeffrey R. Pierce − *Department of Atmospheric Science, Colorado State University, Fort Collins 80525, Colorado, United States;* orcid.org/0000-0002-4241-838X

Complete contact information is available at: https://pubs.acs.org/10.1021/acs.est.0c01345

Author Contributions

A.A., J.R.P., and S.H.J. designed the study. A.A. developed the model and analyzed the results. Y.H. helped with model inputs. M.M.C., A.R.K., K.S., C.W., and J.d.G. provided access to emission data. M.M.C. performed MCM simulations. A.L.H. modeled losses in transfer duct and sampling lines and shared field O/C data. L.Y. and J.H.S. provided access to oxygenated aromatic chamber data. T.B.O., S.C.H., and W.B.K. provided access to measurements made during FIREX. C.D.C. and M.J.K. helped with model development. C.Y.L., J.H.K., and C.D.C. provided access to minichamber data during FIREX. A.A., J.R.P., and S.H.J. wrote the paper with input from all co-authors.

Notes

The authors declare no competing financial interest.

■ ACKNOWLEDGMENTS

This work was supported by the National Oceanic and Atmospheric Administration (NA17OAR4310003, NA17OAR4310001, NA16OAR4310112, and NA16OAR4310111), Colorado Energy Research Collaboratory (37-2018), the Environmental Protection Agency (RD839278), and the National Science Foundation (AGS-1559607). We thank Dr. Manish Shrivastava for useful discussions and Dr. Steven Brown for reviewing this manuscript.

■ REFERENCES

(1) Jimenez, J. L.; Canagaratna, M. R.; Donahue, N. M.; Prevot, A. S. H.; Zhang, Q.; Kroll, J. H.; DeCarlo, P. F.; Allan, J. D.; Coe, H.; Ng, N. L.; Aiken, A. C.; Docherty, K. S.; Ulbrich, I. M.; Grieshop, A. P.; Robinson, A. L.; Duplissy, J.; Smith, J. D.; Wilson, K. R.; Lanz, V. A.; Hueglin, C.; Sun, Y. L.; Tian, J.; Laaksonen, A.; Raatikainen, T.; Rautiainen, J.; Vaattovaara, P.; Ehn, M.; Kulmala, M.; Tomlinson, J. M.; Collins, D. R.; Cubison, M. J.; Dunlea, J.; Huffman, J. A.; Onasch, T. B.; Alfarra, M. R.; Williams, P. I.; Bower, K.; Kondo, Y.; Schneider, J.; Drewnick, F.; Borrmann, S.; Weimer, S.; Demerjian, K.; Salcedo, D.; Cottrell, L.; Griffin, R.; Takami, A.; Miyoshi, T.; Hatakeyama, S.; Shimono, A.; Sun, J. Y.; Zhang, Y. M.; Dzepina, K.; Kimmel, J. R.; Sueper, D.; Jayne, J. T.; Herndon, S. C.; Trimborn, A. M.; Williams, L. R.; Wood, E. C.; Middlebrook, A. M.; Kolb, C. E.; Baltensperger, U.; Worsnop, D. R. Evolution of Organic Aerosols in the Atmosphere. *Science* **2009**, *326*, 1525−1529.

(2) Reid, J. S.; Koppmann, R.; Eck, T. F.; Eleuterio, D. P. A Review of Biomass Burning Emissions Part II: Intensive Physical Properties of Biomass Burning Particles. *Atmos. Chem. Phys.* **2005**, *5*, 799−825.

(3) Lamarque, J.-F.; Bond, T. C.; Eyring, V.; Granier, C.; Heil, A.; Klimont, Z.; Lee, D.; Liousse, C.; Mieville, A.; Owen, B.; Schultz, M. G.; Shindell, D.; Smith, S. J.; Stehfest, E.; Van Aardenne, J.; Cooper, O. R.; Kainuma, M.; Mahowald, N.; McConnell, J. R.; Naik, V.; Riahi, K.; van Vuuren, D. P. Historical (1850−2000) Gridded Anthropogenic and Biomass Burning Emissions of Reactive Gases and Aerosols: Methodology and Application. *Atmos. Chem. Phys.* **2010**, *10*, 7017−7039.

(4) Granier, C.; Bessagnet, B.; Bond, T.; D'Angiola, A.; van der Gon, H. D.; Frost, G. J.; Heil, A.; Kaiser, J. W.; Kinne, S.; Klimont, Z.; Kloster, S.; Lamarque, J.-F.; Liousse, C.; Masui, T.; Meleux, F.; Mieville, A.; Ohara, T.; Raut, J.-C.; Riahi, K.; Schultz, M. G.; Smith, S. J.; Thompson, A.; van Aardenne, J.; van der Werf, G. R.; van Vuuren, D. P. Evolution of Anthropogenic and Biomass Burning Emissions of Air Pollutants at Global and Regional Scales during the 1980−2010 Period. *Clim. Change* **2011**, *109*, 163.

(5) Shrivastava, M.; Cappa, C. D.; Fan, J.; Goldstein, A. H.; Guenther, A. B.; Jimenez, J. L.; Kuang, C.; Laskin, A.; Martin, S. T.; Ng, N. L.; Petaja, T.; Pierce, J. R.; Rasch, P. J.; Roldin, P.; Seinfeld, J. H.; Shilling, J.; Smith, J. N.; Thornton, J. A.; Volkamer, R.; Wang, J.; Worsnop, D. R.; Zaveri, R. A.; Zelenyuk, A.; Zhang, Q. Recent Advances in Understanding Secondary Organic Aerosol: Implications for Global Climate Forcing. *Rev. Geophys.* **2017**, *55*, 509.

(6) McClure, C. D.; Jaffe, D. A. US Particulate Matter Air Quality Improves except in Wildfire-Prone Areas. *Proc. Natl. Acad. Sci. U.S.A.* **2018**, *115*, 7901−7906.

(7) Ford, B.; Val Martin, M.; Zelasky, S. E.; Fischer, E. V.; Anenberg, S. C.; Heald, C. L.; Pierce, J. R. Future Fire Impacts on Smoke Concentrations, Visibility, and Health in the Contiguous United States. *GeoHealth* **2018**, *2*, 229−247.

(8) O'Dell, K.; Ford, B.; Fischer, E. V.; Pierce, J. R. Contribution of Wildland-Fire Smoke to US PM2.5 and Its Influence on Recent Trends. *Environ. Sci. Technol.* **2019**, *53*, 1797−1804.

(9) Hennigan, C. J.; Miracolo, M. A.; Engelhart, G. J.; May, A. A.; Presto, A. A.; Lee, T.; Sullivan, A. P.; McMeeking, G. R.; Coe, H.; Wold, C. E.; Hao, W.-M.; Gilman, J. B.; Kuster, W. C.; de Gouw, J.; Schichtel, B. A.; Collett, J. L., Jr.; Kreidenweis, S. M.; Robinson, A. L. Chemical and Physical Transformations of Organic Aerosol from the Photo-Oxidation of Open Biomass Burning Emissions in an Environmental Chamber. *Atmos. Chem. Phys.* **2011**, *11*, 7669−7686.

(10) Ortega, A. M.; Day, D. A.; Cubison, M. J.; Brune, W. H.; Bon, D.; De Gouw, J. A.; Jimenez, J. L. Secondary Organic Aerosol Formation and Primary Organic Aerosol Oxidation from Biomass-Burning Smoke in a Flow Reactor during FLAME-3. *Atmos. Chem. Phys.* **2013**, *13*, 11551−11571.

(11) Tkacik, D. S.; Robinson, E. S.; Ahern, A.; Saleh, R.; Stockwell, C.; Veres, P.; Simpson, I. J.; Meinardi, S.; Blake, D. R.; Yokelson, R. J.; Presto, A. A.; Sullivan, R. C.; Donahue, N. M.; Robinson, A. L. A Dual-Chamber Method for Quantifying the Effects of Atmospheric Perturbations on Secondary Organic Aerosol Formation from Biomass Burning Emissions: Investigation of Biomass Burning SOA. *J. Geophys. Res., C: Oceans Atmos.* **2017**, *122*, 6043−6058.

(12) Ahern, A. T.; Robinson, E. S.; Tkacik, D. S.; Saleh, R.; Hatch, L. E.; Barsanti, K. C.; Stockwell, C. E.; Yokelson, R. J.; Presto, A. A.; Robinson, A. L.; Sullivan, R. C.; Donahue, N. M. Production of Secondary Organic Aerosol During Aging of Biomass Burning Smoke From Fresh Fuels and Its Relationship to VOC Precursors. *J. Geophys. Res., C: Oceans Atmos.* **2019**, *124*, 3583−3606.

(13) Lim, C. Y.; Hagan, D. H.; Coggon, M. M.; Koss, A. R.; Sekimoto, K.; de Gouw, J.; Warneke, C.; Cappa, C. D.; Kroll, J. H. Secondary Organic Aerosol Formation from the Laboratory Oxidation of Biomass Burning Emissions. *Atmos. Chem. Phys.* **2019**, *19*, 12797−12809.

(14) Jathar, S. H.; Gordon, T. D.; Hennigan, C. J.; Pye, H. O. T.; Pouliot, G.; Adams, P. J.; Donahue, N. M.; Robinson, A. L. Unspeciated Organic Emissions from Combustion Sources and Their Influence on the Secondary Organic Aerosol Budget in the United States. *Proc. Natl. Acad. Sci. U.S.A.* **2014**, *111*, 10473−10478.

(15) Gilman, J. B.; Lerner, B. M.; Kuster, W. C.; Goldan, P. D.; Warneke, C.; Veres, P. R.; Roberts, J. M.; de Gouw, J. A.; Burling, I. R.; Yokelson, R. J. Biomass Burning Emissions and Potential Air Quality Impacts of Volatile Organic Compounds and Other Trace Gases from Fuels Common in the US. *Atmos. Chem. Phys.* **2015**, *15*, 13915−13938.

(16) Hatch, L. E.; Luo, W.; Pankow, J. F.; Yokelson, R. J.; Stockwell, C. E.; Barsanti, K. C. Identification and Quantification of Gaseous Organic Compounds Emitted from Biomass Burning Using Two-Dimensional Gas Chromatography–Time-of-Flight Mass Spectrometry. *Atmos. Chem. Phys.* **2015**, *15*, 1865−1899.
(17) Hatch, L. E.; Yokelson, R. J.; Stockwell, C. E.; Veres, P. R.; Simpson, I. J.; Blake, D. R.; Orlando, J. J.; Barsanti, K. C. Multi-Instrument Comparison and Compilation of Non-Methane Organic Gas Emissions from Biomass Burning and Implications for Smoke-Derived Secondary Organic Aerosol Precursors. *Atmos. Chem. Phys.* **2017**, *17*, 1471−1489.
(18) Hatch, L. E.; Rivas-Ubach, A.; Jen, C. N.; Lipton, M.; Goldstein, A. H.; Barsanti, K. C. Measurements of I/SVOCs in Biomass-Burning Smoke Using Solid-Phase Extraction Disks and Two-Dimensional Gas Chromatography. *Atmos. Chem. Phys.* **2018**, *18*, 17801−17817.
(19) Jen, C. N.; Hatch, L. E.; Selimovic, V.; Yokelson, R. J.; Weber, R.; Fernandez, A. E.; Kreisberg, N. M.; Barsanti, K. C.; Goldstein, A. H. Speciated and Total Emission Factors of Particulate Organics from Burning Western US Wildland Fuels and Their Dependence on Combustion Efficiency. *Atmos. Chem. Phys.* **2019**, *19*, 1013−1026.
(20) Stockwell, C. E.; Veres, P. R.; Williams, J.; Yokelson, R. J. Characterization of Biomass Burning Emissions from Cooking Fires, Peat, Crop Residue, and Other Fuels with High-Resolution Proton-Transfer-Reaction Time-of-Flight Mass Spectrometry. *Atmos. Chem. Phys.* **2015**, *15*, 845−865.
(21) Bruns, E. A.; El Haddad, I.; Slowik, J. G.; Kilic, D.; Klein, F.; Baltensperger, U.; Prévôt, A. S. H. Identification of Significant Precursor Gases of Secondary Organic Aerosols from Residential Wood Combustion. *Sci. Rep.* **2016**, *6*, 27881.
(22) Bruns, E. A.; Slowik, J. G.; El Haddad, I.; Kilic, D.; Klein, F.; Dommen, J.; Temime-Roussel, B.; Marchand, N.; Baltensperger, U.; Prévôt, A. S. H. Characterization of Gas-Phase Organics Using Proton Transfer Reaction Time-of-Flight Mass Spectrometry: Fresh and Aged Residential Wood Combustion Emissions. *Atmos. Chem. Phys.* **2017**, *17*, 705−720.
(23) Koss, A. R.; Sekimoto, K.; Gilman, J. B.; Selimovic, V.; Coggon, M. M.; Zarzana, K. J.; Yuan, B.; Lerner, B. M.; Brown, S. S.; Jimenez, J. L.; Krechmer, J.; Roberts, J. M.; Warneke, C.; Yokelson, R. J.; de Gouw, J. Non-Methane Organic Gas Emissions from Biomass Burning: Identification, Quantification, and Emission Factors from PTR-ToF during the FIREX 2016 Laboratory Experiment. *Atmos. Chem. Phys.* **2018**, *18*, 3299−3319.
(24) Sekimoto, K.; Koss, A. R.; Gilman, J. B.; Selimovic, V.; Coggon, M. M.; Zarzana, K. J.; Yuan, B.; Lerner, B. M.; Brown, S. S.; Warneke, C.; Yokelson, R. J.; Roberts, J. M.; de Gouw, J. High- and Low-Temperature Pyrolysis Profiles Describe Volatile Organic Compound Emissions from Western US Wildfire Fuels. *Atmos. Chem. Phys.* **2018**, *18*, 9263.
(25) Stefenelli, G.; Jiang, J.; Bertrand, A.; Bruns, E. A.; Pieber, S. M.; Baltensperger, U.; Marchand, N.; Aksoyoglu, S.; Prévôt, A. S. H.; Slowik, J. G.; El Haddad, I. Secondary Organic Aerosol Formation from Smoldering and Flaming Combustion of Biomass: A Box Model Parametrization Based on Volatility Basis Set. *Atmos. Chem. Phys.* **2019**, *19*, 11461−11484.
(26) Zhang, X.; Cappa, C. D.; Jathar, S. H.; McVay, R. C.; Ensberg, J. J.; Kleeman, M. J.; Seinfeld, J. H. Influence of Vapor Wall Loss in Laboratory Chambers on Yields of Secondary Organic Aerosol. *Proc. Natl. Acad. Sci. U.S.A.* **2014**, *111*, 5802−5807.
(27) Hodshire, A. L.; Akherati, A.; Alvarado, M. J.; Brown-Steiner, B.; Jathar, S. H.; Jimenez, J. L.; Kreidenweis, S. M.; Lonsdale, C. R.; Onasch, T. B.; Ortega, A. M.; Pierce, J. R. Aging Effects on Biomass Burning Aerosol Mass and Composition: A Critical Review of Field and Laboratory Studies. *Environ. Sci. Technol.* **2019**, *53*, 10007−10022.
(28) He, Y.; King, B.; Pothier, M.; Lewane, L.; Akherati, A.; Mattila, J.; Farmer, D. K.; McCormick, R.; Thornton, M.; Pierce, J. R.; Volckens, J.; Jathar, S. H. Secondary Organic Aerosol Formation from Evaporated Biofuels: Comparison to Gasoline and Correction for Vapor Wall Losses. *Environ. Sci.: Processes Impacts* **2020**, DOI: 10.1039/d0em00103a.
(29) Jathar, S. H.; Cappa, C. D.; Wexler, A. S.; Seinfeld, J. H.; Kleeman, M. J. Simulating secondary organic aerosol in a regional air quality model using the statistical oxidation model - Part 1: Assessing the influence of constrained multi-generational ageing. *Atmos. Chem. Phys.* **2016**, *16*, 2309−2322.
(30) Shiraiwa, M.; Seinfeld, J. H. Equilibration Timescale of Atmospheric Secondary Organic Aerosol Partitioning. *Geophys. Res. Lett.* **2012**, *39* DOI: 10.1029/2012GL054008.
(31) Selimovic, V.; Yokelson, R. J.; Warneke, C.; Roberts, J. M.; de Gouw, J.; Reardon, J.; Griffith, D. W. T. Aerosol Optical Properties and Trace Gas Emissions by PAX and OP-FTIR for Laboratory-Simulated Western US Wildfires during FIREX. *Atmos. Chem. Phys.* **2018**, *18*, 2929−2948.
(32) Koss, A. R.; Sekimoto, K.; Gilman, J. B.; Selimovic, V.; Coggon, M. M.; Zarzana, K. J.; Yuan, B.; Lerner, B. M.; Brown, S. S.; Jimenez, J. L.; Krechmer, J.; Roberts, J. M.; Warneke, C.; Yokelson, R. J.; de Gouw, J. Non-Methane Organic Gas Emissions from Biomass Burning: Identification, Quantification, and Emission Factors from PTR-ToF during the FIREX 2016 Laboratory Experiment. *Atmos. Chem. Phys.* **2018**, *18*, 3299−3319.
(33) Hildebrandt, L.; Donahue, N. M.; Pandis, S. N. High Formation of Secondary Organic Aerosol from the Photo-Oxidation of Toluene. *Atmos. Chem. Phys.* **2009**, *9*, 2973−2986.
(34) Canagaratna, M. R.; Jimenez, J. L.; Kroll, J. H.; Chen, Q.; Kessler, S. H.; Massoli, P.; Hildebrandt Ruiz, L.; Fortner, E.; Williams, L. R.; Wilson, K. R.; Surratt, J. D.; Donahue, N. M.; Jayne, J. T.; Worsnop, D. R. Elemental Ratio Measurements of Organic Compounds Using Aerosol Mass Spectrometry: Characterization, Improved Calibration, and Implications. *Atmos. Chem. Phys.* **2015**, *15*, 253−272.
(35) Rogers, T. M.; Grimsrud, E. P.; Herndon, S. C.; Jayne, J. T.; Kolb, C. E.; Allwine, E.; Westberg, H.; Lamb, B. K.; Zavala, M.; Molina, L. T.; Molina, M. J.; Knighton, W. B. On-Road Measurements of Volatile Organic Compounds in the Mexico City Metropolitan Area Using Proton Transfer Reaction Mass Spectrometry. *Int. J. Mass Spectrom.* **2006**, *252*, 26−37.
(36) Barmet, P.; Dommen, J.; DeCarlo, P. F.; Tritscher, T.; Praplan, A. P.; Platt, S. M.; Prévôt, A. S. H.; Donahue, N. M.; Baltensperger, U. OH Clock Determination by Proton Transfer Reaction Mass Spectrometry at an Environmental Chamber. *Atmos. Meas. Tech.* **2012**, *5*, 647−656.
(37) Cappa, C. D.; Wilson, K. R. Multi-Generation Gas-Phase Oxidation, Equilibrium Partitioning, and the Formation and Evolution of Secondary Organic Aerosol. *Atmos. Chem. Phys.* **2012**, *12*, 9505−9528.
(38) Adams, P. J.; Seinfeld, J. H. Predicting Global Aerosol Size Distributions in General Circulation Models. *J. Geophys. Res., C: Oceans Atmos.* **2002**, *107*, AAC 4−1−AAC 4−23.
(39) Pierce, J. R.; Riipinen, I.; Kulmala, M.; Ehn, M.; Petäjä, T.; Junninen, H.; Worsnop, D. R.; Donahue, N. M. Quantification of the Volatility of Secondary Organic Compounds in Ultrafine Particles during Nucleation Events. *Atmos. Chem. Phys.* **2011**, *11*, 9019−9036.
(40) de Gouw, J.; Warneke, C. Measurements of Volatile Organic Compounds in the Earth's Atmosphere Using Proton-Transfer-Reaction Mass Spectrometry. *Mass Spectrom. Rev.* **2007**, *26*, 223−257.
(41) Coggon, M. M.; Lim, C. Y.; Koss, A. R.; Sekimoto, K.; Yuan, B.; Gilman, J. B.; Hagan, D. H.; Selimovic, V.; Zarzana, K. J.; Brown, S. S.; Roberts, J. M.; Müller, M.; Yokelson, R.; Wisthaler, A.; Krechmer, J. E.; Jimenez, J. L.; Cappa, C.; Kroll, J. H.; de Gouw, J.; Warneke, C. OH Chemistry of Non-Methane Organic Gases (NMOGs) Emitted from Laboratory and Ambient Biomass Burning Smoke: Evaluating the Influence of Furans and Oxygenated Aromatics on Ozone and Secondary NMOG Formation. *Atmos. Chem. Phys.* **2019**, *19*, 14875−14899.
(42) Carlton, A. G.; Bhave, P. V.; Napelenok, S. L.; Edney, E. O.; Sarwar, G.; Pinder, R. W.; Pouliot, G. A.; Houyoux, M. Model

Representation of Secondary Organic Aerosol in CMAQv4.7. *Environ. Sci. Technol.* **2010**, *44*, 8553−8560.
(43) Akherati, A.; Cappa, C. D.; Kleeman, M. J.; Docherty, K. S.; Jimenez, J. L.; Griffith, S. M.; Dusanter, S.; Stevens, P. S.; Jathar, S. H. Simulating Secondary Organic Aerosol in a Regional Air Quality Model Using the Statistical Oxidation Model − Part 3: Assessing the Influence of Semi-Volatile and Intermediate-Volatility Organic Compounds and NO_x. *Atmos. Chem. Phys.* **2019**, *19*, 4561−4594.
(44) Eluri, S.; Cappa, C. D.; Friedman, B.; Farmer, D. K.; Jathar, S. H. Modeling the Formation and Composition of Secondary Organic Aerosol from Diesel Exhaust Using Parameterized and Semi-Explicit Chemistry and Thermodynamic Models. *Atmos. Chem. Phys.* **2018**, *18*, 13813−13838.
(45) Yee, L. D.; Kautzman, K. E.; Loza, C. L.; Schilling, K. A.; Coggon, M. M.; Chhabra, P. S.; Chan, M. N.; Chan, A. W. H.; Hersey, S. P.; Crounse, J. D.; Wennberg, P. O.; Flagan, R. C.; Seinfeld, J. H. Secondary Organic Aerosol Formation from Biomass Burning Intermediates: Phenol and Methoxyphenols. *Atmos. Chem. Phys.* **2013**, *13*, 8019−8043.
(46) Coeur-Tourneur, C.; Cassez, A.; Wenger, J. C. Rate Coefficients for the Gas-Phase Reaction of Hydroxyl Radicals with 2-Methoxyphenol (guaiacol) and Related Compounds. *J. Phys. Chem. A* **2010**, *114*, 11645−11650.
(47) Nakao, S.; Clark, C.; Tang, P.; Sato, K.; Cocker III, D., III. Secondary Organic Aerosol Formation from Phenolic Compounds in the Absence of NO_x. *Atmos. Chem. Phys.* **2011**, *11*, 10649−10660.
(48) Lauraguais, A.; Coeur-Tourneur, C.; Cassez, A.; Deboudt, K.; Fourmentin, M.; Choël, M. Atmospheric Reactivity of Hydroxyl Radicals with Guaiacol (2-Methoxyphenol), a Biomass Burning Emitted Compound: Secondary Organic Aerosol Formation and Gas-Phase Oxidation Products. *Atmos. Environ.* **2014**, *86*, 155−163.
(49) Liu, C.; Liu, J.; Liu, Y.; Chen, T.; He, H. Secondary Organic Aerosol Formation from the OH-Initiated Oxidation of Guaiacol under Different Experimental Conditions. *Atmos. Environ.* **2019**, *207*, 30−37.
(50) Finewax, Z.; de Gouw, J. A.; Ziemann, P. J. Identification and Quantification of 4-Nitrocatechol Formed from OH and NO3 Radical-Initiated Reactions of Catechol in Air in the Presence of NOx: Implications for Secondary Organic Aerosol Formation from Biomass Burning. *Environ. Sci. Technol.* **2018**, *52*, 1981−1989.
(51) Finewax, Z.; de Gouw, J. A.; Ziemann, P. J. Products and Secondary Organic Aerosol Yields from the OH and NO3 Radical-Initiated Oxidation of Resorcinol. *ACS Earth Space Chem.* **2019**, *3*, 1248−1259.
(52) Chhabra, P. S.; Ng, N. L.; Canagaratna, M. R.; Corrigan, A. L.; Russell, L. M.; Worsnop, D. R.; Flagan, R. C.; Seinfeld, J. H. Elemental Composition and Oxidation of Chamber Organic Aerosol. *Atmos. Chem. Phys.* **2011**, *11*, 8827−8845.
(53) Huffman, J. A.; Docherty, K. S.; Mohr, C.; Cubison, M. J.; Ulbrich, I. M.; Ziemann, P. J.; Onasch, T. B.; Jimenez, J. L. Chemically-Resolved Volatility Measurements of Organic Aerosol from Different Sources. *Environ. Sci. Technol.* **2009**, *43*, 5351−5357.
(54) May, A. A.; Levin, E. J. T.; Hennigan, C. J.; Riipinen, I.; Lee, T.; Collett, J. L.; Jimenez, J. L.; Kreidenweis, S. M.; Robinson, A. L. Gas-Particle Partitioning of Primary Organic Aerosol Emissions: 3. Biomass Burning. *J. Geophys. Res., C: Oceans Atmos.* **2013**, *118*, 11327.
(55) Bian, Q.; May, A. A.; Kreidenweis, S. M.; Pierce, J. R. Investigation of Particle and Vapor Wall-Loss Effects on Controlled Wood-Smoke Smog-Chamber Experiments. *Atmos. Chem. Phys.* **2015**, *15*, 11027−11045.
(56) Cappa, C. D.; Lim, C. Y.; Hagan, D. H.; Coggon, M.; Koss, A.; Sekimoto, K.; de Gouw, J.; Onasch, T. B.; Warneke, C.; Kroll, J. Biomass-Burning-Derived Particles from a Wide Variety of Fuels: Part 2: Effects of Photochemical Aging on Particle Optical and Chemical Properties. *Atmos. Chem. Phys.* **2020**, DOI: 10.5194/acp-2020-137.
(57) Grieshop, A. P.; Logue, J. M.; Donahue, N. M. Laboratory Investigation of Photochemical Oxidation of Organic Aerosol from Wood Fires 1: Measurement and Simulation of Organic Aerosol Evolution. *Atmos. Chem. Phys.* **2009**, *9*, 1263.
(58) Takhar, M.; Stroud, C. A.; Chan, A. W. H. Volatility Distribution and Evaporation Rates of Organic Aerosol from Cooking Oils and Their Evolution upon Heterogeneous Oxidation. *ACS Earth Space Chem.* **2019**, *3*, 1717−1728.
(59) Simoneit, B. R. T.; Schauer, J. J.; Nolte, C. G.; Oros, D. R.; Elias, V. O.; Fraser, M. P.; Rogge, W. F.; Cass, G. R. Levoglucosan, a Tracer for Cellulose in Biomass Burning and Atmospheric Particles. *Atmos. Environ.* **1999**, *33*, 173−182.
(60) Aiken, A. C.; Salcedo, D.; Cubison, M. J.; Huffman, J. A.; DeCarlo, P. F.; Ulbrich, I. M.; Docherty, K. S.; Sueper, D.; Kimmel, J. R.; Worsnop, D. R.; Trimborn, A.; Northway, M.; Stone, E. A.; Schauer, J. J.; Volkamer, R. M.; Fortner, E.; de Foy, B.; Wang, J.; Laskin, A.; Shutthanandan, V.; Zheng, J.; Zhang, R.; Gaffney, J.; Marley, N. A.; Paredes-Miranda, G.; Arnott, W. P.; Molina, L. T.; Sosa, G.; Jimenez, J. L. Mexico City Aerosol Analysis during MILAGRO Using High Resolution Aerosol Mass Spectrometry at the Urban Supersite (T0) − Part 1: Fine Particle Composition and Organic Source Apportionment. *Atmos. Chem. Phys.* **2009**, *9*, 6633−6653.
(61) Cubison, M. J.; Ortega, A. M.; Hayes, P. L.; Farmer, D. K.; Day, D.; Lechner, M. J.; Brune, W. H.; Apel, E.; Diskin, G. S.; Fisher, J. A.; Fuelberg, H. E.; Hecobian, A.; Knapp, D. J.; Mikoviny, T.; Riemer, D.; Sachse, G. W.; Sessions, W.; Weber, R. J.; Weinheimer, A. J.; Wisthaler, A.; Jimenez, J. L. Effects of Aging on Organic Aerosol from Open Biomass Burning Smoke in Aircraft and Laboratory Studies. *Atmos. Chem. Phys.* **2011**, *11*, 12049−12064.
(62) Krechmer, J. E.; Pagonis, D.; Ziemann, P. J.; Jimenez, J. L. Quantification of Gas-Wall Partitioning in Teflon Environmental Chambers Using Rapid Bursts of Low-Volatility Oxidized Species Generated in Situ. *Environ. Sci. Technol.* **2016**, *50*, 5757−5765.
(63) Lu, Q.; Zhao, Y.; Robinson, A. L. Comprehensive Organic Emission Profiles for Gasoline, Diesel, and Gas-Turbine Engines Including Intermediate and Semi-Volatile Organic Compound Emissions. *Atmos. Chem. Phys.* **2018**, *18*, 17637−17654.
(64) Atkinson, R.; Arey, J. Atmospheric Degradation of Volatile Organic Compounds. *Chem. Rev.* **2003**, *103*, 4605−4638.
(65) Joo, T.; Rivera-Rios, J. C.; Takeuchi, M.; Alvarado, M. J.; Ng, N. L. Secondary Organic Aerosol Formation from Reaction of 3-Methylfuran with Nitrate Radicals. *ACS Earth Space Chem.* **2019**, *3*, 922−934.
(66) McClure, C. D.; Lim, C. Y.; Hagan, D. H.; Kroll, J. H.; Cappa, C. D. Biomass-Burning-Derived Particles from a Wide Variety of Fuels − Part 1: Properties of Primary Particles. *Atmos. Chem. Phys.* **2020**, *20*, 1531−1547.
(67) Shrivastava, M.; Cappa, C. D.; Fan, J.; Goldstein, A. H.; Guenther, A. B.; Jimenez, J. L.; Kuang, C.; Laskin, A.; Martin, S. T.; Ng, N. L.; Petaja, T.; Pierce, J. R.; Rasch, P. J.; Roldin, P.; Seinfeld, J. H.; Shilling, J.; Smith, J. N.; Thornton, J. A.; Volkamer, R.; Wang, J.; Worsnop, D. R.; Zaveri, R. A.; Zelenyuk, A.; Zhang, Q. Recent advances in understanding secondary organic aerosol: Implications for global climate forcing. *Rev. Geophys.* **2017**, *55*, 509−559.
(68) Garofalo, L. A.; Pothier, M. A.; Levin, E. J. T.; Campos, T.; Kreidenweis, S. M.; Farmer, D. K. Emission and Evolution of Submicron Organic Aerosol in Smoke from Wildfires in the Western United States. *ACS Earth Space Chem.* **2019**, *3*, 1237.
(69) Hodshire, A. L.; Campuzano-Jost, P.; Kodros, J. K.; Croft, B.; Nault, B. A.; Schroder, J. C.; Jimenez, J. L.; Pierce, J. R. The Potential Role of Methanesulfonic Acid (MSA) in Aerosol Formation and Growth and the Associated Radiative Forcings. *Atmos. Chem. Phys.* **2019**, *19*, 3137−3160.
(70) Ramnarine, E.; Kodros, J. K.; Hodshire, A. L.; Lonsdale, C. R.; Alvarado, M. J.; Pierce, J. R. Effects of near-Source Coagulation of Biomass Burning Aerosols on Global Predictions of Aerosol Size Distributions and Implications for Aerosol Radiative Effects. *Atmos. Chem. Phys.* **2019**, *19*, 6561−6577.
(71) Liu, X.; Huey, L. G.; Yokelson, R. J.; Selimovic, V.; Simpson, I. J.; Müller, M.; Jimenez, J. L.; Campuzano-Jost, P.; Beyersdorf, A. J.; Blake, D. R.; Butterfield, Z.; Choi, Y.; Crounse, J. D.; Day, D. A.; Diskin, G. S.; Dubey, M. K.; Fortner, E.; Hanisco, T. F.; Hu, W.; King,

L. E.; Kleinman, L.; Meinardi, S.; Mikoviny, T.; Onasch, T. B.; Palm, B. B.; Peischl, J.; Pollack, I. B.; Ryerson, T. B.; Sachse, G. W.; Sedlacek, A. J.; Shilling, J. E.; Springston, S.; St. Clair, J. M.; Tanner, D. J.; Teng, A. P.; Wennberg, P. O.; Wisthaler, A.; Wolfe, G. M. Airborne Measurements of Western U.S. Wildfire Emissions: Comparison with Prescribed Burning and Air Quality Implications. *J. Geophys. Res., C: Oceans Atmos.* **2017**, *122*, 6108−6129.

(72) Sengupta, D.; Samburova, V.; Bhattarai, C.; Watts, A. C.; Moosmüller, H.; Khlystov, A. Y. Polar Semi-Volatile Organic Compounds in Biomass Burning Emissions and Their Chemical Transformations during Aging in an Oxidation Flow Reactor. *Atmos. Chem. Phys. Discuss.* **2020**, DOI: 10.5194/acp-2019-1179.

(73) Smith, J. D.; Sio, V.; Yu, L.; Zhang, Q.; Anastasio, C. Secondary Organic Aerosol Production from Aqueous Reactions of Atmospheric Phenols with an Organic Triplet Excited State. *Environ. Sci. Technol.* **2014**, *48*, 1049−1057.

(74) Yu, L.; Smith, J.; Laskin, A.; Anastasio, C.; Laskin, J.; Zhang, Q. Chemical Characterization of SOA Formed from Aqueous-Phase Reactions of Phenols with the Triplet Excited State of Carbonyl and Hydroxyl Radical. *Atmos. Chem. Phys.* **2014**, *14*, 13801−13816.

(75) Huang, Y.; Zhao, R.; Charan, S. M.; Kenseth, C. M.; Zhang, X.; Seinfeld, J. H. Unified Theory of Vapor−Wall Mass Transport in Teflon-Walled Environmental Chambers. *Environ. Sci. Technol.* **2018**, *52*, 2134−2142.

(76) Cappa, C. D.; Jathar, S. H.; Kleeman, M. J.; Docherty, K. S.; Jimenez, J. L.; Seinfeld, J. H.; Wexler, A. S. Simulating Secondary Organic Aerosol in a Regional Air Quality Model Using the Statistical Oxidation Model–Part 2: Assessing the Influence of Vapor Wall Losses. *Atmos. Chem. Phys.* **2016**, *16*, 3041−3059.

(77) Lim, Y. B.; Ziemann, P. J. Chemistry of Secondary Organic Aerosol Formation from OH Radical-Initiated Reactions of Linear, Branched, and Cyclic Alkanes in the Presence of NOx. *Aerosol Sci. Technol.* **2009**, *43*, 604−619.

(78) Presto, A. A.; Miracolo, M. A.; Donahue, N. M.; Robinson, A. L. Secondary Organic Aerosol Formation from High-NOx Photo-Oxidation of Low Volatility Precursors: N-Alkanes. *Environ. Sci. Technol.* **2010**, *44*, 2029−2034.

(79) Forstner, H. J. L.; Flagan, R. C.; Seinfeld, J. H. Secondary Organic Aerosol from the Photooxidation of Aromatic Hydrocarbons: Molecular Composition. *Environ. Sci. Technol.* **1997**, *31*, 1345−1358.

(80) Griffin, R. J.; Cocker, D. R., III; Seinfeld, J. H.; Dabdub, D. Estimate of Global Atmospheric Organic Aerosol from Oxidation of Biogenic Hydrocarbons. *Geophys. Res. Lett.* **1999**, *26*, 2721−2724.

(81) Keywood, M. D.; Varutbangkul, V.; Bahreini, R.; Flagan, R. C.; Seinfeld, J. H. Secondary Organic Aerosol Formation from the Ozonolysis of Cycloalkenes and Related Compounds. *Environ. Sci. Technol.* **2004**, *38*, 4157−4164.

■ NOTE ADDED AFTER ASAP PUBLICATION

This paper was published ASAP on July 6, 2020, with errors in the Supporting Information. The corrected version was reposted on July 21, 2020.

https://dx.doi.org/10.1021/acs.est.0c01345
Environ. Sci. Technol. 2020, 54, 8568−8579